*Proceedings of the 3rd World Congress on Civil, Structural, and Environmental Engineering (CSEE'18)*
*Budapest, Hungary – April 8 - 10, 2018*
*Paper No. ICGRE 153*
*DOI: 10.11159/icgre18.153*

# Effect of the Cross-Sectional Rigidity on the Static and Seismic Behaviour of CSP Culverts

**Ahmed Mahgoub, Hany El Naggar**
Dalhousie University
1360 Barrington Street, Halifax, NS, Canada
ahmed.mahgoub@dal.ca; hany.elnaggar@dal.ca

***Abstract –*** In Canada and around the world there is a growing trend to use wide span soil-steel arch structures as a substitute for the more conventional types of bridges and rigid culverts. CSP culverts (corrugated steel plate culverts) are flexible structures which gain load-bearing capacity by interaction with the surrounding engineered backfill enabling them to carry significant overburden and vehicular loads. In this paper, comprehensive finite element analyses were carried out to study the effect of changing the cross-sectional rigidity on the static and seismic behaviour of CSP culverts. First, the static behaviour of a field case study of a wide span culvert was verified. Then, the full dynamic analyses were utilized using seismic records suitable for the city of Vancouver in Western Canada. Subsequently, the culvert's cross-sectional properties were changed to examine their effect on the culvert's performance. Finally, the results of the finite element analyses were compared with the simplified design equations of the Canadian Highway Bridge Design Code (CHBDC). This study shows that the culvert's cross-sectional rigidity has a significant effect on the soil structure interaction (SSI) between the culvert and the surrounding backfill, which affects the performance and the load carrying capacity of the culvert.

***Keywords*:** CSP Arch Culverts, Soil-Steel System, Seismic Hazards, Seismic Performance, Canadian Highway Bridge Design Code (CHBDC).

## 1. Introduction

Over the past 50 years, corrugated steel plate (CSP) arch culverts have proved to be a practical solution for various river crossings in Canada, US and around the world and have been used for several railway/highway overpass structures [1]. Buried arches are usually used for railway and highway underpasses (such as tunnels) built using the cut and cover method, or for culverts and arch bridges. The buried arch tunnels are very advantageous as they can also be used as short to medium span bridges [2].

The behaviour of long-span deep corrugated metal culverts is significantly affected by many factors. These factors are influenced mainly by the manner in which the loads will spread through the soil before reaching the tunnel. This, in turn, is governed by the burial depth of the structure; the rise and span of the tunnel; the number of design lanes (i.e. the number of trucks acting on the structure); and the designed positions of the trucks at the surface [3].

In the last few decades, the industrial development of corrugated steel plates was proliferating. Only shallow corrugated plates with 51mm height and 152mm pitch and deep corrugated plates with 140mm height and 381mm pitch were used in the design of various applications [4]. Also, stiffening rib products were also manufactured to improve the structural stiffness. Recently in 2010, the deeper corrugated plate (237mm height and 500mm pitch) was introduced into the market [4]. The static design equations of steel buried arches/culverts in the CHBDC consider only the single radius steel structures with shallow corrugations and with a maximum width of up to 20.0 m. Moreover, The code was developed utilizing arches with spans varying from 6.0 to 20.0 m and soil cover not more than 50% of the span width [5].

Numerous studies have been conducted to study the seismic design of underground structures [6-11], but few covered the performance of buried flexible culverts and large span culverts. While the previously mentioned studies showed that if the foundation conditions are stable, and have not been affected by the earthquake, the culvert should not be subject to significant seismic loads, hence, it is suitable to use the simplified seismic design equations of the code. Mahgoub and El Naggar [12] studied the seismic performance of CSP culverts in the city of Victoria, Canada, under different earthquake magnitudes. They reported that the moment and thrust at the springlines experience a notable change during earthquakes

and they govern the design in this case, whereas the design in the code is governed by the straining actions at the crown location.

Synthetic time history records were created by many studies [13-17] to be compatible with the targeted uniform hazard spectrum (UHS) according to the National Building Code of Canada (NBCC, 2015). Atkinson [18] reported that the simulated records are developed for Western Canada according to the site condition, earthquake magnitude and the fault distances. Atkinson developed five sets for different earthquake magnitudes [18]. Every set has 45 random records at different fault location for every site condition to represent the earthquake in the specific region. These records were used in this study to select suitable time history records for the city of Vancouver in Canada.

In this study, finite element (FE) analyses were carried out to study the effect of changing the cross-sectional rigidity of the CSP buried arches on their static and seismic performance. Subsequently, the FE results were compared with the design by the simplified equations in the CHBDC to assess its suitability.

## 2. Methodology

The FE model, which was developed in [12] to verify the monitored field case study in [19], was used in this study. Also, the site response analyses were conducted to select the proper scaled artificial time history proposed by [18] that is suitable for the city of Vancouver, Canada. Then, the effect of the cross-sectional rigidity on the static and seismic behaviour of the CSP was examined by changing the arch's cross-section considering shallow, deep and deeper corrugations. Finally, the FE results were compared with the results of the CHBDC's simplified equations.

## 3. Verified Field Test

As mentioned in [12], a detailed two-dimensional finite element model using PLAXIS 2017 was developed to verify the well-documented case study presented in [19]. The model simulated the construction sequence and accounted for the soil-structure interaction including the effects of the compaction of the backfill around the culvert. The results of the model upon completion of backfilling and before the application of live loads were compared to the experimental test results. Fig. 1 shows the layout of the verified case study. Moreover, Fig. 2 (a) illustrated the comparison between the measured bending moments in the field test at the locations of the crown and the curvature change location (near the shoulder), respectively, and the results of the FE model under static loading conditions. Also, Fig. 2 (b) presents the comparison of the vertical deformations at the same locations. More details of this FE model can be found in [12].

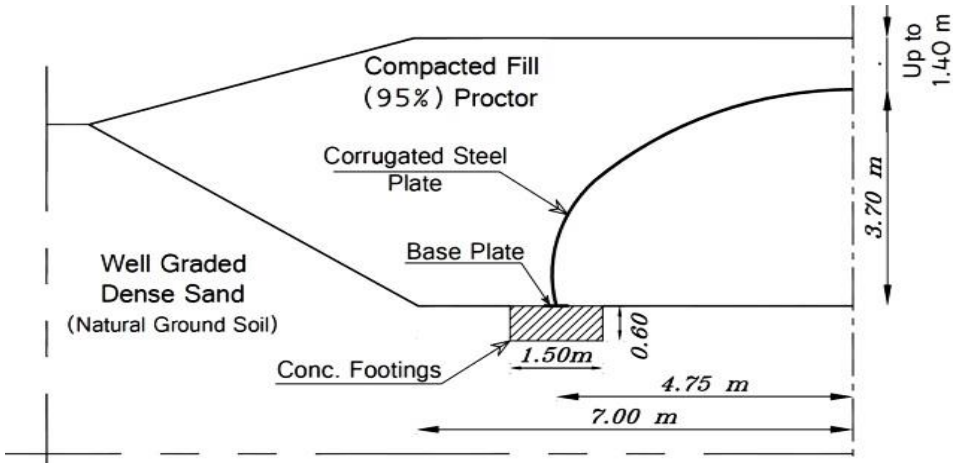


Fig. 1: Steel arch geometry [19].

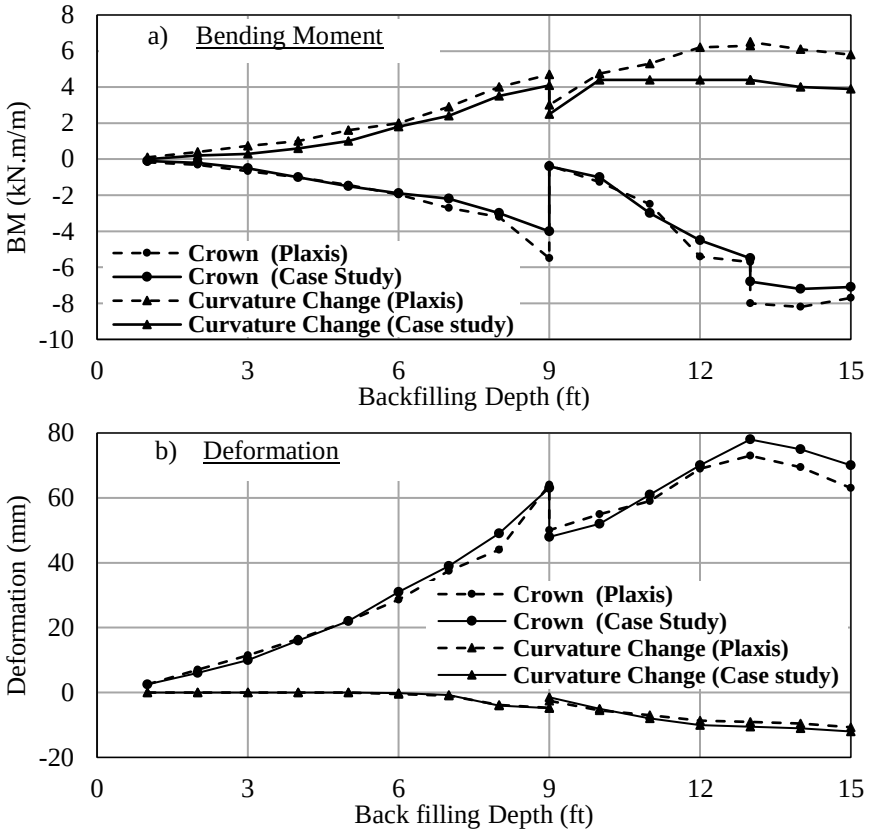


Fig. 2: Comparison between the measured field test and the FE model results, a) bending moment, and b) deformations [12].

## 4. Site Response Analysis

1D finite element models were carried out to select/ obtain appropriate site-specific time histories for the city of Vancouver for site C conditions, as the in-situ material of the verified field test was well-graded sand with gravel (SW), per ASTM D 2487, with 1% fines. Seismic waves will propagate from the source (which is considered to be at the bedrock level) up to ground level. The characteristics of the seismic wave are modified when it travels through soil deposits, which acts as a filter. As suggested by Atkinson [18], the sets M6.5 (R from 10 to 20) is recommended for high hazard regions in Western Canada. Therefore, the analyses using these records were carried out to find the compatible time history to the targeted UHS.

### 4.1. Geometry

The models were developed utilizing 40 m of homogeneous soil (Site C). Fig. 3 shows the geometry of the model. The spectrum was estimated at the ground surface was compared and scaled to the targeted spectrum in NBCC 2015. The model width is depending on the wave propagation and velocity which will be discussed in the next section. 45 records were tried to find the most appropriate record to be used in the full dynamic analyses.

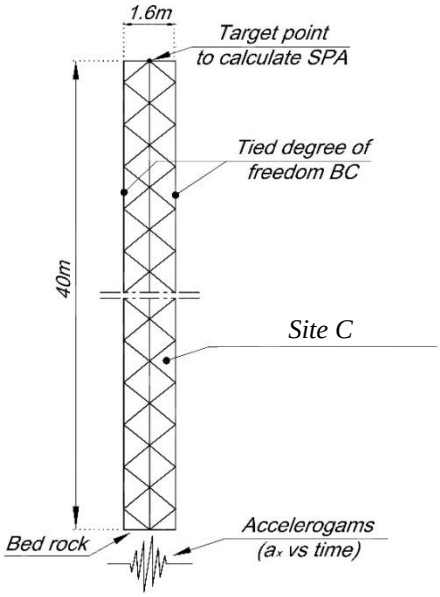

Fig. 3: Geometry of the 1D- seismic analysis model.

### 4.2. Finite Element Mesh

The soil was modelled using the 15-noded triangular plain strain element from the PLAXIS library. This element provides more accurate results as it follows a higher order interpolation function [20]. The mesh was adjusted to comply with equation (1) [21]:

$$\lambda/8 = (Vs, min)/(8 * f\max) \quad (1)$$

Where $V_{s\ min}$ is the lowest shear wave velocity in the soil profile and $f_{max}$ is the maximum frequency component of the inserted wave which can be calculated from Fourier spectrum analysis.

### 4.3. Soil model

The soil medium was modelled using the Hardening Soil Small Strain (HS-Small) soil model. In the HS-Small model, the small strain stiffness relation is implemented according to the formulation in [22]. The unloading/reloading stiffness of the HS-Small model has a nonlinear dependency of the strain utilizing the 'small strain overlay model' [22]. The overlay model is based on the modulus reduction curve, formed by the shear modulus, G and the shear strain, $\gamma$. This relationship between G and $\gamma$ can be identified by the cyclic triaxial test or by various other relationships as shown in the literature [23]. Table 1 presents the soil parameters of Site C which were selected according to the natural ground surface in the case study [19]. The small strain shear modulus $G_0$ was estimated using the correlation in [23].

Table 1: The used soil parameters.

| Material | φ' | E | $E_{oed}$ | $E_{ur}$ | ɣ | c | $G_0$ |
|---|---|---|---|---|---|---|---|
| | 0 | MPa | MPa | MPa | KN/m$^3$ | kPa | MPa |
| In-situ soil | 43 | 40 | 32 | 120 | 20 | 0 | 200 |

### 4.4. Damping

In PLAXIS, The Damping Matrix (C) = $\alpha$ M +$\beta$ K, where M is the mass matrix and K is the stiffness matrix. Also, Rayleigh Damping scalers ($\alpha$, $\beta$) were added for target frequencies 1 and 2 to define the damping behaviour of the soil.

$$\alpha + \beta\ \omega^2 = 2\omega\xi \ \text{ and } \omega = 2\pi\ F \quad (2)$$

Two targeted frequencies ($F_1$ and $F_2$) should be identified. $F_1$ is the fundamental frequency of the soil layer which is given by:

$$F_1 = \frac{V_s}{4H} \tag{3}$$

Where Vs is the average soil shear velocity according to the site type. $F_2$ is the closest integral odd number given by the ratio between the fundamental frequency of the input signal (By Fourier Spectrum) and the fundamental frequency of the soil layer [24].

### 4.5. Boundary Conditions

In the case of one-dimensional wave propagation, the option tied degree of freedom allows modeling a reduced geometry of the problem. It is sufficient to define the soil column by the horizontal dimension defined according to the average element size, while the nodes at the left and the right of the model boundary are connected with each other and are characterized by the same displacement [20].

### 4.6. Results and Discussion of the Site Response Analysis

Fig. 4 shows the simulated response spectrum of the scaled records for site C compared with the targeted spectrum in NBCC 2015 within the various period ranges of interest (0.1 to 1 Second). The used amplification factor is 0.75.

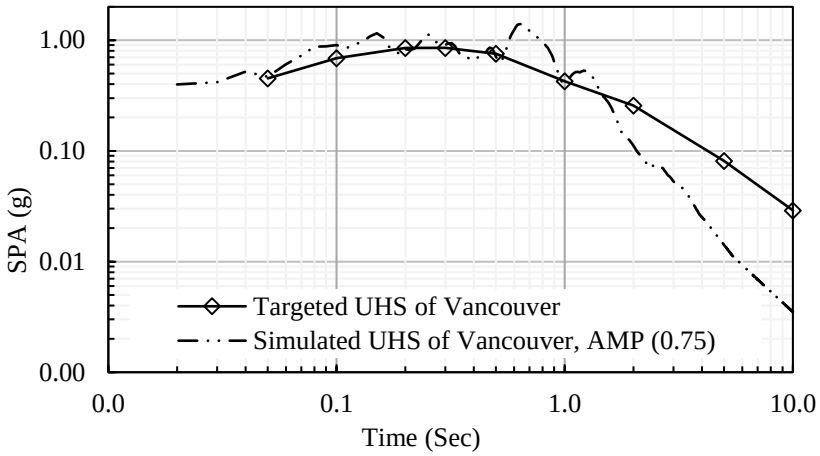


Fig. 4: NBCC 2015 targeted spectrum compared to selected scaled record.

## 5. Development of FE model for CSP culvert

Fig. 5 shows the main geometry of the adopted two-dimensional finite element model including the mesh formulation and different simulated parts, i.e., the CSP culvert, backfill, interface, and the concrete footings. Three FE Models were developed by utilizing different cross-sections (i.e. shallow, deep and deeper corrugation) to understand the effect of cross-section's rigidity on the seismic and static performance of the CSP culverts. The same geometry and materials properties were followed as per the case study. Same assumptions in the material models (Section 4.3) are followed in the complete model by using Hardening soil model with small strain. The backfilling material properties are selected according to the results of the Hyperbolic model in [19]. Table 2 shows the used properties of the backfilling material. The natural ground and the backfilling envelope were modelled using higher order 15-node triangular elements. The model has around 12,000 elements with an average element size of 180 mm. The large number of small-sized elements assured high accuracy, especially at locations where nonlinear behaviour was expected (e.g. in close vicinity to the culvert).

Table 2: The used backfill parameters [21].

| The property index | Value | units |
|---|---|---|
| φ’ | 41 | ° |
| E | 33 | MPa |
| $E_{oed}$ | 26.4 | MPa |
| $E_{ur}$ | 99 | MPa |
| ɣ | 18.50 | KN/$m^3$ |
| c | 0 | kPa |
| $G_0$ | 128 | MPa |
| $\gamma_{0.7}$ | 0.15e-3 | --- |
| $P_{ref}$ | 41 | kPa |

In addition, the same considerations which are mentioned in section 4.2 for the meshing should be utilized in the complete model. The reinforced concrete footings were modelled as a volume element using an elastic material model. Additionally, the steel plates were modelled utilizing an isotropic elastic material. The steel plate properties used in the model were obtained from [19], as shown in Table 3. The base plate, which is used to fix the steel arches to the concrete footing, is a horizontal steel plate with 5 mm thickness and 300 mm width.

Interface elements were placed between the CSP arches and the backfilling layers. The roughness of the interaction was modelled by utilizing a strength-reduction factor at the interface $R_{inter}$ = 0.67. Similarly, the interface elements were installed between the concrete footings and the soil layers with $R_{inter}$= 0.67.

Table 3: Steel and concrete properties [20].

| Material | E (GPa) | Passion’s Ratio | Inertia ($mm^4$/mm) |
|---|---|---|---|
| Concrete (Foundation) | 30 | 0.15 | ---- |
| *Steel (Shallow Corrugation) | 200 | 0.3 | 2079.8 |
| **Steel (Deep Corrugation) | | | 24124.5 |
| **Steel (Deeper Corrugation) | | | 97031.45 |

*cross-section used in the considered cased study

**cross-sections considered in the parametric study according to ASTM (A796)

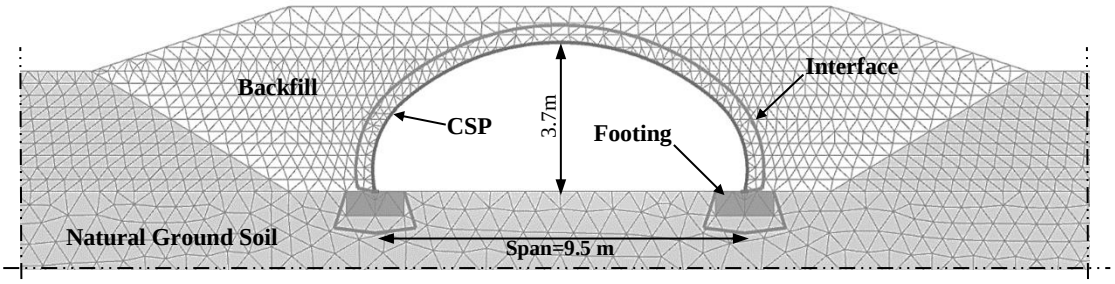


Fig. 5: The adopted FE mesh.

Sensitivity analyses were conducted to specify the model lateral dimensions and the types of the boundary conditions. Accordingly, the free field boundary conditions were utilized in the analyses with 120 m width.

## 6. Results and Discussion

In this section, the results of the finite element models are presented and compared with the results of the simplified equations in the CHBDC under the static and the seismic loading conditions, respectively. Even though the FE results included the accompanied thrust and bending moments at the base, Springline, shoulder and crown of the

culvert, the Code's equations give only the thrust forces at the base and the bending moments at the crown. Fig. 6 shows the thrust forces and bending moments distributions around the culvert under the static loading condition. The figure illustrates that there is a significant effect of changing the culvert's rigidity on the bending moment's distribution. Where the maximum bending moment in the culvert with shallow corrugations was at the crown. While it was located at the springline in the culvert with deep and deeper corrugations. Moreover, it can be seen from the same figure that the maximum thrust forces usually were encountered at the base.

Fig. 7 shows the effect of the culvert's stiffness and rigidity on the seismic straining actions. It can be seen from this Figure that the thrust increases with increasing the culvert's rigidity, where the maximum thrust at the base were 230, 244 and 248 kN/m for the developed models with shallow, deep and deeper corrugation, respectively. This increase in the thrust is negligible and will have no significant implications on the design. While there is a significant increase of the bending moment as the cross-section got stiffer as can be seen from the figure, as, the maximum bending moments were 28, 80 and 124 kN.m/m for models with cross-sections made from shallow, deep and deeper corrugated plates, respectively.

On the other hand, it can be seen from Fig. 6 that there is a good agreement between thrust forces under the static loading condition obtained from the FE models and the design equations of the CHBDC in all models. While a significant change in the bending moment values was found, it can be seen that the maximum bending moment by the design equations in CHBDC were 7.55, 7.55 and 11.05 kN.m/m for shallow, deep and deeper corrugations, respectively. While, the FE results calculated 7.9, 7 and 18 kN.m/m for the same cross-sections respectively.

In addition, Fig. 7 reveals that the bending moment at the crown due to the seismic loading estimated using the CHBDC's equations is 9.7, 9.7 and 13.7 kN.m/m for shallow, deep and deeper corrugations. While, the maximum bending moments were 28, 80 and 124 kN.m/m respectively for the same cross-sections as calculated by the FE analyses. It can be clearly noticed from the figures that the simplified equations underestimate the straining actions for the designs. Thus, for cities located in zones of high seismicity, the simplified equations are not recommended, and a rigorous finite element analysis is required. Also, the design equations under the static loading conditions should be deeply investigated before being applied for stiff cross-sections.

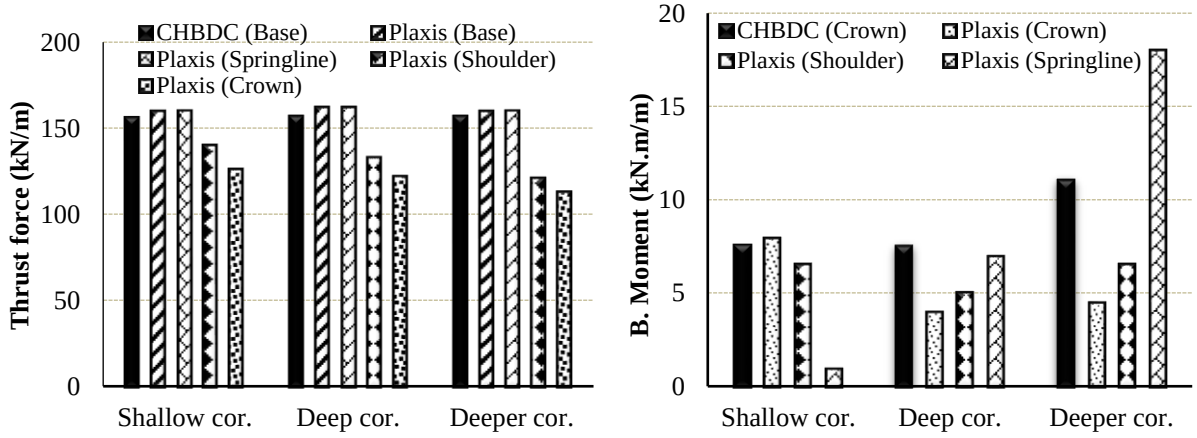


Fig. 6: Thrust forces and bending moments under static loading conditions.

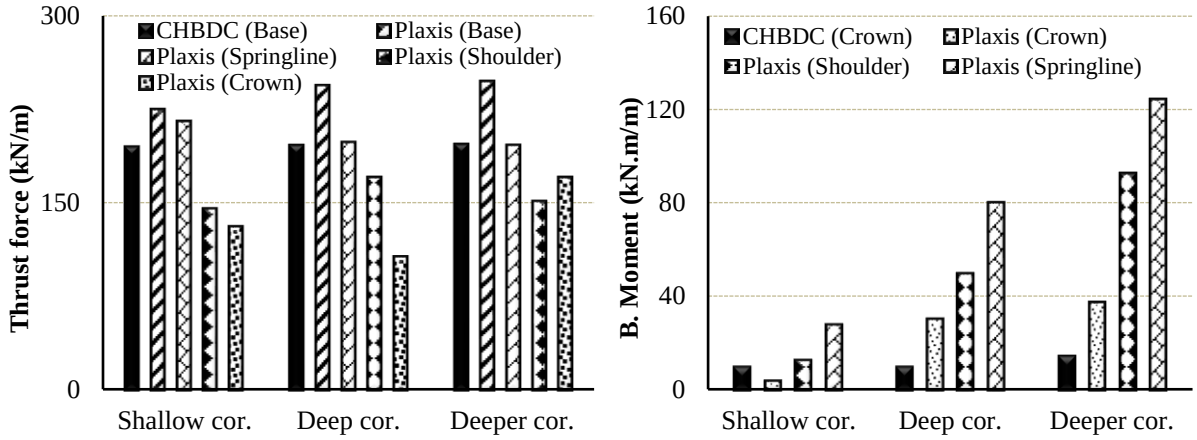


Fig. 7: Thrust forces and bending moments under the seismic loading conditions.

## 7. Conclusion

A detailed two-dimensional finite element study was conducted to investigate the effect of cross-sectional rigidity on the performance of CSP culverts under both static and seismic loading conditions. The study involved developing models that simulated the construction sequence and accounted for the soil-structure interaction including the effects of the compaction of the backfill around the culvert. The following conclusions can be drawn based on the results of the study:

1.This study showed that the cross-section's rigidity has a significant effect on the culvert's performance under both static and seismic loading conditions.

2.The culvert's rigidity has a significant effect on the bending moment's distribution around the culvert under static conditions. The maximum bending moment in the culvert with shallow corrugations was at the crown, while, it was located at the springline in the culverts with deep and deeper corrugations

3.For low profile culverts, the straining actions at the springlines experience a notable change during earthquakes, and they govern the design in this case.

4.The CHBDC's design equations should be deeply investigated and revised to be applied in high seismicity zones.

**References**

[1] D. Kolymbas, Tunnelling and Tunnel Mechanics: A Rational Approach to Tunnelling. Springer Science & Business Media, 2005.

[2] T. J. McGrath, I. D. Moore, E. T. Selig, M. C. Webb and B. Taleb, "Design Examples For Large-Span Culverts: Nchrp Report 473," 2002.

[3] T. M. Elshimi, R. W. Brachman and I. D. Moore, "Effect of truck position and multiple truck loading on response of long-span metal culverts," *Canadian Geotechnical Journal*, vol. 51, no. 2, pp. 196-207, 2013.

[4] J. H. Fortin Vallée, "Investigation of Increased Wall Stiffness on Load Effect Equations for Soil Metal Structures," 2015.

[5] D. Choi, G. Kim and P. M. Byrne, "Evaluation of moment equation in the 2000 Canadian highway bridge design code for soil–metal arch structures," *Canadian Journal of Civil Engineering*, vol. 31, no. 2, pp. 281-291, 2004.

[6] A. Hindy and M. Novak, "Earthquake response of underground pipelines," *Earthquake Eng. Struct. Dyn*., vol. 7, no. 5, pp. 451-476, 1979.

[7] C. A. Davis and J. P. Bardet, "Seismic analysis of large-diameter flexible underground pipes," J. Geotech. Geoenviron. Eng., vol. 124, no. 10, pp. 1005-1015, 1998.

[8] C. A. Davis and J. P. Bardet, "Responses of buried corrugated metal pipes to earthquakes," *J. Geotech. Geoenviron. Eng.*, vol. 126, no. 1, pp. 28-39, 2000.

[9] Y. M. Hashash, J. J. Hook, B. Schmidt, I. John and C. Yao, "Seismic design and analysis of underground structures," Tunnel. Underground Space Technol., vol. 16, no. 4, pp. 247-293, 2001.
[10] P. Byrne, D. Anderson and H. Jitno, "Seismic analysis of large buried culvert structures," *Transportation Research Record: Journal of the Transportation Research Board*, vol. 1541, pp. 133-139, 1996.
[11] T. L. Youd and C. J. Beckman, "Highway culvert performance during past earthquakes (no. NCEER-96-0015)," 1996.
[12] A. Mahgoub, H. El Naggar, "Assessment of the seismic provisions of the CHBDC for CSP culverts," in *GeoOttawa 2017, the 70th Canadian Geotechnical Conference*, 2017.
[13] D. Motazedian and G. M. Atkinson, "Stochastic finite-fault modeling based on a dynamic corner frequency," *Bulletin of the Seismological Society of America*, vol. 95, no. 3, pp. 995-1010, 2005.
[14] G. M. Atkinson and D. M. Boore, "Earthquake ground-motion prediction equations for eastern North America," *Bulletin of the Seismological Society of America*, vol. 96, no. 6, pp. 2181-2205, 2006.
[15] K. Assatourians and G. M. Atkinson, "Modeling variable-stress distribution with the stochastic finite-fault technique," *Bulletin of the Seismological Society of America*, vol. 97, no. 6, pp. 1935-1949, 2007.
[16] D. M. Boore and G. M. Atkinson, "Ground-motion prediction equations for the average horizontal component of PGA, PGV, and 5%-damped PSA at spectral periods between 0.01 s and 10.0 s," Earthquake Spectra, vol. 24, no. 1, pp. 99-138, 2008.
[17] M. Macias, G. M. Atkinson and D. Motazedian, "Ground-motion attenuation, source, and site effects for the 26 September 2003 M 8.1 Tokachi-Oki earthquake sequence," *Bulletin of the Seismological Society of America*, vol. 98, no. 4, pp. 1947-1963, 2008.
[18] G. M. Atkinson, "Earthquake time histories compatible with the 2005 National building code of Canada uniform hazard spectrum," *Canadian Journal of Civil Engineering*, vol. 36, no. 6, pp. 991-1000, 2009.
[19] M. C. Webb, E. T. Selig and T. J. McGrath, "Instrumentation for monitoring large-span culverts," in *Field Instrumentation for Soil and Rock Anonymous ASTM International*, 1999.
[20] B. PLAXIS, *Reference Manual for PLAXIS 2D*, 2017.
[21] R. L. Kuhlemeyer and J. Lysmer, "Finite element method accuracy for wave propagation problems," *Journal of Soil Mechanics & Foundations Div*, vol. 99, 1973.
[22] T. Benz, "Small-Strain Stiffness of Soils and its Numerical Consequences, Mitteilung des Instituts for Geotechnik der Universitat Stuttgart," Germany. Stuttgart, 2006.
[23] H. B. Seed, "Soil moduli and damping factors for dynamic response analysis report no. EERC 70-10," 1970.
[24] M. Hudson, I. M. Idriss and M. Beirkae, "QUAD4M user's manual," 1994.